PHYSICAL REVIEW D **78,** 083520 (2008)

# Interpreting the recent results on direct searches for dark matter particles in terms of relic neutralinos

A. Bottino,[1] F. Donato,[1] N. Fornengo,[1] and S. Scopel[2]

[1]*Dipartimento di Fisica Teorica, Università di Torino, Istituto Nazionale di Fisica Nucleare, Sezione di Torino, via P. Giuria 1, I-10125 Torino, Italy*

[2]*Korea Institute for Advanced Study, Seoul 130-722, Korea*

(Received 10 July 2008; published 13 October 2008)

The most recent results from direct searches for dark matter particles in the Galactic halo are examined in terms of an effective minimal supersymmetric extension of the standard model at the electroweak scale without unification of gaugino masses. We show that the annual-modulation effect at $8.2\sigma$ C.L. recently presented by the DAMA Collaboration, as the result of a combined analysis of the DAMA/NaI and the DAMA/LIBRA experiments for a total exposure of 0.82 ton yr, fits remarkably well with what is expected for relic neutralinos for a wide variety of weakly interacting massive particle distribution functions. Bounds derivable from other measurements of direct searches for dark matter particles are analyzed. We stress the role played by the uncertainties affecting the neutralino-quark couplings arising from the involved hadronic quantities. We also examine how present data on cosmic antiprotons can help in constraining the neutralino configurations selected by the DAMA effect, in connection with the values of the astrophysical parameters. Perspectives for measurements of antideuterons, possibly produced in the Galactic halo by self-annihilation of neutralinos belonging to the DAMA configurations, are examined. Finally, we discuss how findings at the LHC would impact on these issues.

DOI: 10.1103/PhysRevD.78.083520 PACS numbers: 95.35.+d, 11.30.Pb, 12.60.Jv, 95.30.Cq

## I. INTRODUCTION

We are at present witnessing great activity in running and preparing experimental projects of direct searches for dark matter (DM) particles in the Galactic halo [1].

A number of new results appeared recently. Most notably, the DAMA Collaboration, by analyzing the data obtained with the DAMA/LIBRA experiment [2], has confirmed the evidence for the annual-modulation effect already measured with the previous DAMA/NaI experiment [3]. As a result of the combined analysis of the DAMA/NaI and the DAMA/LIBRA experiments, for a total exposure of 0.82 ton yr, the effect of the annual modulation is now at $8.2\sigma$ C.L. [2]. Other collaborations have reported upper bounds on the WIMP-nucleon scalar cross section [1,4–6] (as usual, here WIMP stands for a generic weakly interacting massive particle), using other approaches and scaling from different nuclei.

In this paper we discuss the relevance of these experimental results for the most widely discussed candidate for cold dark matter, the neutralino. Neutralino configurations (concerning here mainly light neutralinos) which fit the annual-modulation data are extracted from the DAMA results and confronted with the current measurements on Galactic antiprotons. Perspectives of seeing signals due to these configurations in forthcoming measurements of Galactic antideuterons are examined. The current experimental upper bounds on the WIMP-nucleon scalar cross section are also scrutinized.

In all our considerations we explicitly take into account the uncertainties affecting the neutralino-quark couplings because of the involved hadronic quantities, typically the pion-nucleon sigma term $\sigma_{\pi N}$, the quantity $\sigma_0$ which is related to the SU(3) symmetry breaking, and a quark mass ratio $r$ (see definitions later on).

In the analysis of the DAMA data, we discuss both the case in which the channeling effect [7] is included in their analysis and the one where this effect is not taken into account; these two cases are treated separately. We recall that the channeling effect occurs when an ion, traversing a crystalline structure along a path (quasi-) parallel to crystallographic axes or planes, has a deeper penetration than in an amorphous material of the same composition [8]. In Ref. [7] it is shown that the occurrence of the channeling effect makes the response of the DAMA NaI(Tl) detector more sensitive to WIMP-nucleus interactions than previously estimated.

Finally, in the present paper it is stressed that the CERN LHC (Large Hadron Collider), which hopefully will shed light on the Higgs sector and supersymmetric extensions of the standard model (SM), has a remarkable discovery potential in terms of the population of light neutralinos which fit the annual-modulation data.

The plan of the paper is the following. In Sec. II the main features of the supersymmetric model employed in the present paper are delineated. Section III is devoted to a recollection of the main phenomenological properties used in our analysis, and Secs. IV and V to a detailed comparison of our theoretical evaluations to the current results of WIMP direct detection. In Sec. VI we discuss the constraints implied by measurements of Galactic antiprotons, and in Sec. VII we examine the perspectives for forth-

 

coming measurements on cosmic antideuterons. The impact of the LHC on these issues is discussed in Sec. VIII, and finally conclusions are drawn in Sec. IX.

## II. THE SUPERSYMMETRIC MODEL

The supersymmetric scheme we employ in the present paper is the one described in Ref. [9], an effective minimal supersymmetric extension of the standard model (effMSSM) at the electroweak scale, with the following independent parameters: $M_1$, $M_2$, $\mu$, $\tan\beta$, $m_A$, $m_{\tilde{q}}$, $m_{\tilde{l}}$, and $A$. Notations are as follows: $M_1$ and $M_2$ are the U(1) and SU(2) gaugino masses (these parameters are taken here to be positive), $\mu$ is the Higgs mixing mass parameter, $\tan\beta$ is the ratio of the two Higgs vacuum expectation values, $m_A$ is the mass of the $CP$-odd neutral Higgs boson, $m_{\tilde{q}}$ is a squark soft-mass common to all squarks, $m_{\tilde{l}}$ is a slepton soft-mass common to all sleptons, and $A$ is a common dimensionless trilinear parameter for the third family, $A_{\tilde{b}} = A_{\tilde{t}} \equiv A m_{\tilde{q}}$ and $A_{\tilde{\tau}} \equiv A m_{\tilde{l}}$ (the trilinear parameters for the other families being set equal to zero). In our model, no gaugino-mass unification at a grand-unified-theory scale is assumed. The lightest neutralino is required to be the lightest supersymmetric particle and to be stable (because of $R$-parity conservation).

In the present paper the numerical analyses are performed by a scanning of the supersymmetric parameter space, with the following ranges of MSSM parameters: $1 \leq \tan\beta \leq 50$, $100\ \text{GeV} \leq |\mu| \leq 1000\ \text{GeV}$, $5\ \text{GeV} \leq M_1 \leq 500\ \text{GeV}$, $100\ \text{GeV} \leq M_2 \leq 1000\ \text{GeV}$, $100\ \text{GeV} \leq m_{\tilde{q}}$, $m_{\tilde{l}} \leq 3000\ \text{GeV}$, $90\ \text{GeV} \leq m_A \leq 1000\ \text{GeV}$, $-3 \leq A \leq 3$.

The following experimental constraints are imposed: accelerator data on supersymmetric and Higgs boson searches (the CERN $e^+e^-$ collider LEP2 [10] and Collider Detectors D0 and CDF at Fermilab [11]); measurements of the $b \to s + \gamma$ decay process [12] [$2.89 \leq B(b \to s + \gamma) \times 10^{-4} \leq 4.21$ is employed here]—this interval is larger by 25% with respect to the experimental determination [12] in order to take into account theoretical uncertainties in the supersymmetric contributions [13] to the branching ratio of the process (for the standard model calculation, we employ the recent next-to-next-to-leading order results from Ref. [14]); the upper bound on the branching ratio $\text{BR}(B_s^0 \to \mu^- + \mu^+)$ [15] [we take $\text{BR}(B_s^0 \to \mu^- + \mu^+) < 1.2 \times 10^{-7}$]; and measurements of the muon anomalous magnetic moment $a_\mu \equiv (g_\mu - 2)/2$ (for the deviation $\Delta a_\mu$ of the experimental world average from the theoretical evaluation within the standard model, we use here the range $-98 \leq \Delta a_\mu \times 10^{11} \leq 565$, derived from the latest experimental [16] and theoretical [17] data).

Also included is the cosmological constraint that the neutralino relic abundance does not exceed the maximal allowed value for cold dark matter, i.e. $\Omega_\chi h^2 \leq (\Omega_{\text{CDM}} h^2)_{\text{max}}$. We set $(\Omega_{\text{CDM}} h^2)_{\text{max}} = 0.122$, as derived at a $2\sigma$ level from the results of Ref. [18]. We recall that this cosmological upper bound implies, on the neutralino mass, the lower limit $m_\chi \gtrsim 7$ GeV [9].

## III. PHENOMENOLOGY RELATED TO THE DIRECT SEARCH OF GALACTIC WIMPS

In the case of WIMPs with coherent interactions with nuclei, the differential event rate $dR/dE_R$ ($E_R$ being the nuclear recoil energy) measured in WIMP direct searches can be written as

$$\frac{dR}{dE_R} = N_T \frac{\rho_0}{m_\chi} \frac{m_N}{2\mu_1^2} A^2 \xi \sigma_{\text{scalar}}^{(\text{nucleon})} F^2(E_R) \mathcal{I}(v_{\text{min}}), \quad (1)$$

where

$$\mathcal{I}(v_{\text{min}}) = \int_{w \geq v_{\text{min}}} d^3 w \frac{f_{\text{ES}}(\vec{w})}{w}. \quad (2)$$

In these formulas, the notations are as follows: $N_T$ is the number of target nuclei per unit mass, $m_N$ is the nucleus mass, $\mu_1$ is the WIMP-*nucleon* reduced mass, $A$ is the nuclear mass number, $\sigma_{\text{scalar}}^{(\text{nucleon})}$ is the WIMP-nucleon coherent cross section, $F(E_R)$ is the nuclear form factor, $\xi$ is the fraction of the mass density of the WIMP in terms of the total local density for nonbaryonic dark matter $\rho_0$ (i.e. $\xi = \rho_W/\rho_0$), $f_{\text{ES}}(\vec{w})$ and $\vec{w}$ denote the velocity distribution function (DF) and WIMP velocity in the Earth frame, respectively ($w = |\vec{w}|$), and $v_{\text{min}}$ is the minimal Earth-frame WIMP velocity which contributes to a given recoil energy $E_R$: $v_{\text{min}} = [m_N E_R/(2\mu_A^2)]^{1/2}$ ($\mu_A$ being the WIMP-*nucleus* reduced mass).

It is convenient to define a velocity distribution function in the Galactic rest frame $f(\vec{v})$, where $\vec{v} = \vec{w} + \vec{v}_\oplus$, $\vec{v}_\oplus$ being the Earth's velocity in the Galactic rest frame. The Earth-frame velocity DF is then obtained by means of the transformation $f_{\text{ES}}(\vec{w}) = f(\vec{w} + \vec{v}_\oplus)$. By definition, the velocity distribution function $f(\vec{v})$ is given by the six-dimensional phase-space distribution function $F(\vec{r}, \vec{v})$ evaluated at the Earth's location $\vec{R}_0$ in the Galaxy, i.e. $f(\vec{v}) = F(\vec{R}_0, \vec{v})$. The velocity DF $f(\vec{v})$ is truncated at a maximal escape velocity $v_{\text{esc}}$, since the gravitational field of the Galaxy cannot bound arbitrarily fast WIMPs.

By employing Eqs. (1) and (2) one can derive information on the quantity $\xi \sigma_{\text{scalar}}^{(\text{nucleon})}$ from the measurements on the differential rate $dR/dE_R$, once a specific velocity distribution function $f(\vec{v})$ is selected.

### A. WIMP distribution functions

A systematic study of various distribution functions was carried out in Ref. [19], and a number of these DFs were subsequently analyzed in Ref. [20] to study the sensitivity of the upper bounds on $\xi \sigma_{\text{scalar}}^{(\text{nucleon})}$ derived from different experiments of WIMP direct detection.

In Ref. [19] the phase-space DFs were classified into four categories, depending on the symmetry properties of the matter density (or the corresponding gravitational potential) and of the velocity dependence: A) spherically symmetric matter density $\rho_{\rm DM}$ with isotropic velocity dispersion, B) spherically symmetric matter density with nonisotropic velocity dispersion, C) axisymmetric models, D) triaxial models [21,22]. For each category, different specific models are identified.

In Ref. [19] a procedure was developed to determine, for each individual velocity DF, the relevant range of the $\rho_0$ values. Specifically, each halo model was constrained by a number of observational inputs: (i) properties of the Galactic rotational curve, namely, the range of the allowed values for the local rotational velocity, 170 km sec$^{-1}$ $\leq v_0 \leq$ 270 km sec$^{-1}$ [23,24], and the amount of flatness of the rotational curve at large distances from the Galactic center, and (ii) the maximal amount of nonhalo components in the Galaxy, $M_{\rm vis}$ (i.e. the disk, the bulge, etc.). These constraints determine the extremes of the local dark matter density $\rho_0$. For instance, when one assumes a maximal halo (i.e. the contribution of the nonhalo components is minimized) $\rho_0$ is maximal, and on the contrary, the value of $\rho_0$ is minimal when the contribution of the halo to the rotational curve is minimal. By this procedure, for any specific analytic form of the velocity DF and any value of the local rotational velocity $v_0$ within the interval 170 km sec$^{-1}$ $\leq v_0 \leq$ 270 km sec$^{-1}$, one derives the relevant lower and upper bounds, $\rho_0^{\rm min}$ and $\rho_0^{\rm max}$, for the local DM density. Obviously, $\rho_0^{\rm min}$ and $\rho_0^{\rm max}$ are increasing functions of $v_0$, since a large amount of local matter is necessary to support a large value of the local rotational velocity.

Notice that both $\rho_0$ and $v_0$ are crucial parameters in establishing the properties of the quantity $\xi\sigma_{\rm scalar}^{\rm (nucleon)}$, when this is extracted from the detection rate. Whereas $\rho_0$ has the role of a normalization factor, $v_0$ is related to both the WIMP kinetic energy and to the change in the reference frames, and thus is crucial in determining the shapes of the sensitivity levels usually reported in the plane $m_\chi$—$\xi\sigma_{\rm scalar}^{\rm (nucleon)}$.

In the present paper, as our reference model we take the cored-isothermal sphere, which we will discuss in detail; we will also comment about some other DFs. The density profile of the cored-isothermal sphere (denoted as the Evans logarithmic model, or the A1 model, in Ref. [19]) is

$$\rho(r) = \frac{v_0^2}{4\pi G}\,\frac{3R_c^2 + r^2}{(R_c^2 + r^2)^2}, \tag{3}$$

where $G$ is Newton's constant, $v_0$ is the local value of the rotational velocity, and $R_c$ is the core radius. For $R_c$ we use the value $R_c = 5$ kpc. For the parameter $v_0$ we will consider the values $v_0 = 170, 220, 270$ km sec$^{-1}$, which represent the minimal, central, and maximal values of $v_0$ in its physical range. For these values of $v_0$, the extreme values of $\rho_0$ are as follows: (i) $v_0 = 170$ km sec$^{-1}$ with $\rho_0^{\rm min} = 0.20$ GeV cm$^{-3}$ and $\rho_0^{\rm max} = 0.42$ GeV cm$^{-3}$; (ii) $v_0 = 220$ km sec$^{-1}$ with $\rho_0^{\rm min} = 0.34$ GeV cm$^{-3}$ and $\rho_0^{\rm max} = 0.71$ GeV cm$^{-3}$; (iii) $v_0 = 270$ km sec$^{-1}$ with $\rho_0^{\rm min} = 0.62$ GeV cm$^{-3}$ and $\rho_0^{\rm max} = 1.07$ GeV cm$^{-3}$.

### B. Local fractional density

The WIMP fractional density $\xi = \rho_W/\rho_0$ is taken to be $\xi = \min\{1, \Omega_\chi h^2/(\Omega_{\rm CDM}h^2)_{\rm min}\}$, in order to have rescaling [25], when $\Omega_\chi h^2$ turns out to be less than $(\Omega_{\rm CDM}h^2)_{\rm min}$ [here $(\Omega_{\rm CDM}h^2)_{\rm min}$ is set to the value 0.098, as derived at a $2\sigma$ level from the results of Ref. [18].]

### C. WIMP-nucleon cross section: Hadronic uncertainties

The neutralino-nucleon scalar cross section $\sigma_{\rm scalar}^{\rm (nucleon)}$ is mainly due to exchanges of the two $CP$-even neutral Higgs bosons, $h$ and $H$, in the $t$ channel [26] and to squark exchanges in the $s$ and $u$ channels [27]. The expression of $\sigma_{\rm scalar}^{\rm (nucleon)}$ may be found in [28].

In the cross section representing the Higgs exchanges, the factors involving the couplings between the Higgs bosons and the nucleon may be written as $I_{h,H} = \sum_q k_q^{h,H} m_q \langle N|\bar{q}q|N\rangle$, where the coefficients $k_q^{h,H}$ depend on supersymmetric parameters, $\langle N|\bar{q}q|N\rangle$ denotes the scalar density of the quark $q$ in the nucleon, and $m_q$ is the quark mass. The coefficients $k_q^{h,H}$ are given in [29].

The calculation of the quantities $m_q\langle N|\bar{q}q|N\rangle$ is usually carried out by first expressing these quantities in terms of the pion-nucleon sigma term,

$$\sigma_{\pi N} = \tfrac{1}{2}(m_u + m_d)\langle N|\bar{u}u + \bar{d}d|N\rangle, \tag{4}$$

of the quantity $\sigma_0$, related to the size of the SU(3) symmetry breaking,

$$\sigma_0 \equiv \tfrac{1}{2}(m_u + m_d)\langle N|\bar{u}u + \bar{d}d - 2\bar{s}s|N\rangle, \tag{5}$$

and of the ratio $r = 2m_s/(m_u + m_d)$.

In fact, by assuming isospin invariance for quarks $u$ and $d$, the quantities $m_q\langle N|\bar{q}q|N\rangle$ for light quarks may be written as

$$m_u\langle N|\bar{u}u|N\rangle \simeq m_d\langle N|\bar{d}d|N\rangle \simeq \tfrac{1}{2}\sigma_{\pi N}, \tag{6}$$

$$m_s\langle N|\bar{s}s|N\rangle \simeq \tfrac{1}{2}r(\sigma_{\pi N} - \sigma_0). \tag{7}$$

As for the heavy quarks $c$, $b$, $t$, one conveniently employs the heavy quark expansion [30] to obtain

$$m_c\langle N|\bar{c}c|N\rangle \simeq m_b\langle N|\bar{b}b|N\rangle \simeq m_t\langle N|\bar{t}t|N\rangle \simeq \frac{2}{27}\left[m_N - \sigma_{\pi N} + \frac{1}{2}r(\sigma_{\pi N} - \sigma_0)\right], \tag{8}$$

where $m_N$ is the nucleon mass.

In this way the quantities $I_{h,H}$ can be reexpressed as

$$I_{h,H} = k^{h,H}_{u\text{-type}} g_u + k^{h,H}_{d\text{-type}} g_d, \tag{9}$$

where

$$g_u \simeq m_l \langle N|\bar{l}l|N\rangle + 2m_h \langle N|\bar{h}h|N\rangle \simeq \frac{4}{27}\left(m_N + \frac{19}{8}\sigma_{\pi N} - \frac{1}{2} r(\sigma_{\pi N} - \sigma_0)\right), \tag{10}$$

$$g_d \simeq m_l \langle N|\bar{l}l|N\rangle + m_s \langle N|\bar{s}s|N\rangle + m_h \langle N|\bar{h}h|N\rangle \simeq \frac{2}{27}\left(m_N + \frac{23}{4}\sigma_{\pi N} + \frac{25}{4} r(\sigma_{\pi N} - \sigma_0)\right); \tag{11}$$

$l$ stands for light quarks ($l = u, d$) and $h$ denotes the heavy ones ($h = c, b, t$).

The major problem here is that the three quantities $\sigma_{\pi N}$, $\sigma_0$, and $r$ are all affected by sizable uncertainties which in turn dramatically affect the determination of the coefficients $g_u$ and $g_d$. This problem was stressed in Refs. [29,31] (see also Refs. [32,33] for earlier discussions of this point) and subsequently also recognized by other authors [34–38].

The range of $\sigma_{\pi N}$ we considered in Ref. [31] was

$$41 \text{ MeV} \lesssim \sigma_{\pi N} \lesssim 57 \text{ MeV} \tag{12}$$

as derived from the pion-nucleon scattering amplitude, calculated at the so-called Cheng-Dashen point by Koch [39], and from the evolution of the nucleon scalar form factor, as a function of the momentum transfer from $t = 2m_\pi^2$ to $t = 0$, evaluated in Ref. [40].

In Ref. [29] we reconsidered the calculation of the coefficients $g_u$, $g_d$ in light of a new determination of $\sigma_{\pi N}$ presented in Ref. [41]. In fact, the George Washington University/TRIUMF group, using updated pion-nucleon scattering data [42] and a new partial-wave and dispersion relation analysis program, derived a range for $\sigma_{\pi N}$ [41],

$$55 \text{ MeV} \lesssim \sigma_{\pi N} \lesssim 73 \text{ MeV}, \tag{13}$$

which turned out to be sizably larger than the one in Eq. (12). Values of the nucleon scalar form factor at the Cheng-Dashen point higher than those of Ref. [39] were also reported in Ref. [43].

In Ref. [29] we stressed the dramatic importance that the uncertainties in the hadronic quantities $\sigma_{\pi N}$, $\sigma_0$, and $r$ have in a number of fundamental issues, namely, (i) evaluation of WIMP detection rates in direct and also in some indirect searches (neutrino fluxes due to WIMP self-annihilation in the Earth and the Sun), (ii) actual regions of the supersymmetric parameter space involved in searches for WIMPs, and (iii) connection between experimental event rates and relic abundance.

It is unfortunate that the dichotomy between the two determinations in Eq. (12) and in Eq. (13) still persists. This fact is not only related to the experimental determination of the relevant quantities in the pion-nucleon scattering, but also to the intricacies involved in the derivation of $\sigma_{\pi N}$ from the experimental data. It is worth noting that the uncertainty inherent in the value of $\sigma_{\pi N}$ could be even larger than the one exemplified by Eqs. (12) and (13) (see Ref. [44] for further determinations).

For definiteness, in the present paper we consider variations of $\sigma_{\pi N}$ in the range which is the union of the two intervals of Eqs. (12) and (13), i.e.

$$41 \text{ MeV} \lesssim \sigma_{\pi N} \lesssim 73 \text{ MeV}. \tag{14}$$

In the presentation of our results, we will also consider a reference point, representative of a value of $\sigma_{\pi N}$ which is within the narrow overlap of the two ranges of Eqs. (12) and (13).

The quantity $\sigma_0$ is taken in the range [45]

$$\sigma_0 = 30 \div 40 \text{ MeV} \tag{15}$$

and the *default* value $r = 25$ is assigned to the mass ratio $r = 2m_s/(m_u + m_d)$.

We recall that the fractional strange-quark content of the nucleon $y$,

$$y = 2\frac{\langle N|\bar{s}s|N\rangle}{\langle N|\bar{u}u + \bar{d}d|N\rangle}, \tag{16}$$

is linked to $\sigma_0$ and $\sigma_{\pi N}$ by the expression

$$y = 1 - \frac{\sigma_0}{\sigma_{\pi N}}. \tag{17}$$

The reference point mentioned above, meant to represent an estimate of the hadronic quantities in agreement with both ranges of Eqs. (12) and (13), is defined by the values $g_{u,\text{ref}} = 123$ MeV, $g_{d,\text{ref}} = 290$ MeV (this set of values is the one employed also in our previous paper, Ref. [46]). As mentioned above, together with this representative point, we will also explicitly discuss the implications of the full range of $\sigma_{\pi N}$ given in Eq. (14).

## IV. THE ANNUAL-MODULATION EFFECT MEASURED BY THE DAMA COLLABORATION

The first results of the DAMA/LIBRA experiment on direct detection of dark matter particles have recently been presented [2]. These data concern an exposure of 0.53 ton yr. When added to the previous exposure of 0.29 ton yr of the DAMA/NaI experiment [3], the total exposure collected by the DAMA Collaboration, with the DAMA/LIBRA and the DAMA/NaI experiments together, amounts to 0.82 ton yr. The analysis of the total set of data shows an annual-modulation effect in the event rate at $8.2\sigma$ C.L. This yearly modulation satisfies all the features expected for an annual variation due to relic particles in our Galactic halo [47] and is not explained by systematic effects and/or seasonal variations of other various origins [2].

The relic particles responsible for the DAMA annual-modulation effect can be of many different kinds; a number of possible candidates are recollected in Ref. [2] (see e.g. also [48–51]). In the present paper we analyze the interpretation of the DAMA effect in terms of relic neutralinos.

Indeed, we already invoked neutralinos [52] since the very first DAMA results of Ref. [53] which showed a yearly variation in the direct signal. Our interpretation was further pursued, most notably in Refs. [9,54,55], where the focus was on light neutralinos (i.e. neutralinos with masses $m_\chi \lesssim 50$ GeV).

More recently, we presented a new investigation of the DAMA/NaI results [46], when the DAMA Collaboration discussed the possible implications of including the channeling effect in the analysis of their data [7].

In this paper we update our interpretation of the annual-modulation effect in light of the experimental results improved by the quite sizable increase in total exposure of the recent DAMA experiments.

From now on, when mentioning DAMA data we will mean the total set of data including both the DAMA/NaI experiment and the DAMA/LIBRA one, reported in Ref. [2].

In the following section we will discuss the annual-modulation regions, in the plane $m_\chi - \xi\sigma_{\rm scalar}^{\rm (nucleon)}$ ($m_\chi$ denotes the WIMP mass), that have been derived by the DAMA Collaboration for the case of a WIMP with a coherent interaction with nuclei [56]. The derivation has been carried out both in the case where the channeling effect is taken into account and in the one where channeling is not included. We recall that the features of the annual-modulation region in the plane $m_\chi - \xi\sigma_{\rm scalar}^{\rm (nucleon)}$ depend sensitively on the specific model-dependent procedure employed in the evaluation of the channeling effect. The regions reported hereby for the case of channeling correspond to the case where channeling is included with the model explained in Ref. [7]. Actually, the extent to which the channeling effect occurs when a putative WIMP traverses a NaI crystal is still under study. For this reason,

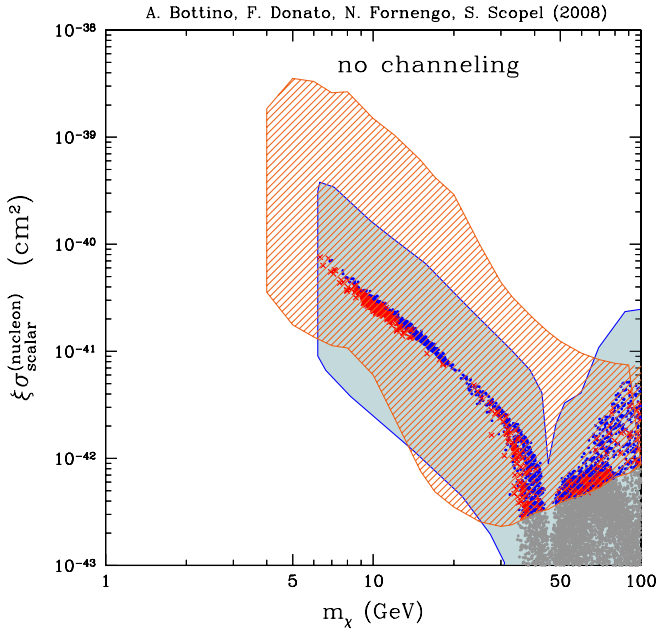


FIG. 1 (color online). $\xi\sigma_{\rm scalar}^{\rm (nucleon)}$ as a function of the WIMP mass. The region covered by a (red) slant hatching denotes the DAMA annual-modulation region, under the hypothesis that the effect is due to a WIMP with a coherent interaction with nuclei and *without including* the channeling effect. This region represents the domain where the likelihood-function values differ by more than $6.5\sigma$ from the null hypothesis (absence of modulation). It has been derived by the DAMA Collaboration by varying the WIMP Galactic distribution function over the set considered in Ref. [19] and by taking into account other uncertainties of different origins [57]. The scatter plot represents supersymmetric configurations calculated with the model summarized in Sec. II, at the fixed representative set of values for the hadronic quantities characterized by $g_{u,\rm ref} = 123$ MeV, $g_{d,\rm ref} = 290$ MeV. The (red) crosses denote configurations with a neutralino relic abundance which matches the WMAP cold dark matter amount ($0.098 \leq \Omega_\chi h^2 \leq 0.122$), while the (blue) dots refer to configurations where the neutralino is subdominant ($\Omega_\chi h^2 < 0.098$). The (blue) uniformly shaded region represents the extension of the scatter plot upwards and downwards, when the hadronic uncertainties reported in Eq. (14) are included (see text).

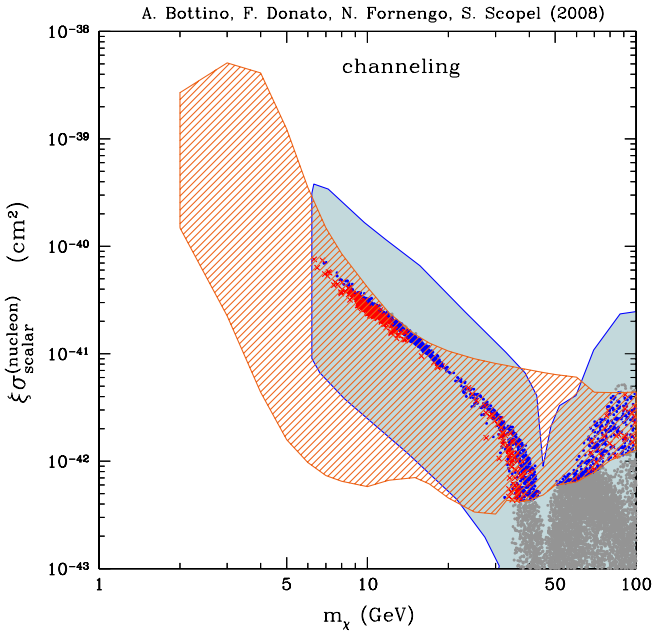


FIG. 2 (color online). $\xi\sigma_{\rm scalar}^{\rm (nucleon)}$ as a function of the WIMP mass. The region covered by a (red) slant hatching denotes the DAMA annual-modulation region, under the hypothesis that the effect is due to a WIMP with a coherent interaction with nuclei and *including* the channeling effect. All other prerequisites of this region are as in Fig. 1. The scatter plot and the (blue) uniformly shaded region are as in Fig. 1.

in our analysis we consider both cases of no channeling and of channeling with the model of Ref. [7]. One expects that the actual physical situation is comprised within these two cases.

### A. Annual-modulation regions (convolution over a class of distribution functions)

We start our analysis by showing in Figs. 1 and 2 the DAMA annual-modulation regions in a plot of $\xi\sigma_{\rm scalar}^{\rm (nucleon)}$ versus the WIMP mass. These have been derived by the DAMA Collaboration for the case of a WIMP with a coherent interaction with nuclei [56], by varying the WIMP Galactic DF over the set considered in Ref. [19] and by taking into account other uncertainties of different origins [57]. The DAMA regions are denoted by a (red) slant hatching; they represent regions where the likelihood-function values differ more than $6.5\sigma$ from the null hypothesis (absence of modulation). Figure 1 refers to the case in which the channeling effect is not included, whereas Fig. 2 displays the case where channeling is included.

Figures 1 and 2 also show the (blue) uniformly shadowed region, which represents the physical neutralino region as derived within our effective MSSM. The scatter plot, common to Figs. 1 and 2, denotes the results of our evaluations, when a scanning over the supersymmetric parameter space is performed, at the fixed representative set of values for the hadronic quantities mentioned in Sec. III C. This representative set is characterized by the values $g_{u,\rm ref} = 123$ MeV, $g_{d,\rm ref} = 290$ MeV (we recall that this set is the one employed also in our previous paper, Ref. [46]). The (red) crosses and the (blue) dots of the scatter plot denote configurations with no rescaling and those with rescaling of the local density, respectively (see Sec. III B). The features of the supersymmetric configurations belonging to the scatter plot are discussed in detail in Ref. [9].

The uniformly shaded region displayed in Figs. 1 and 2 represents the extension of the scatter plot upwards and

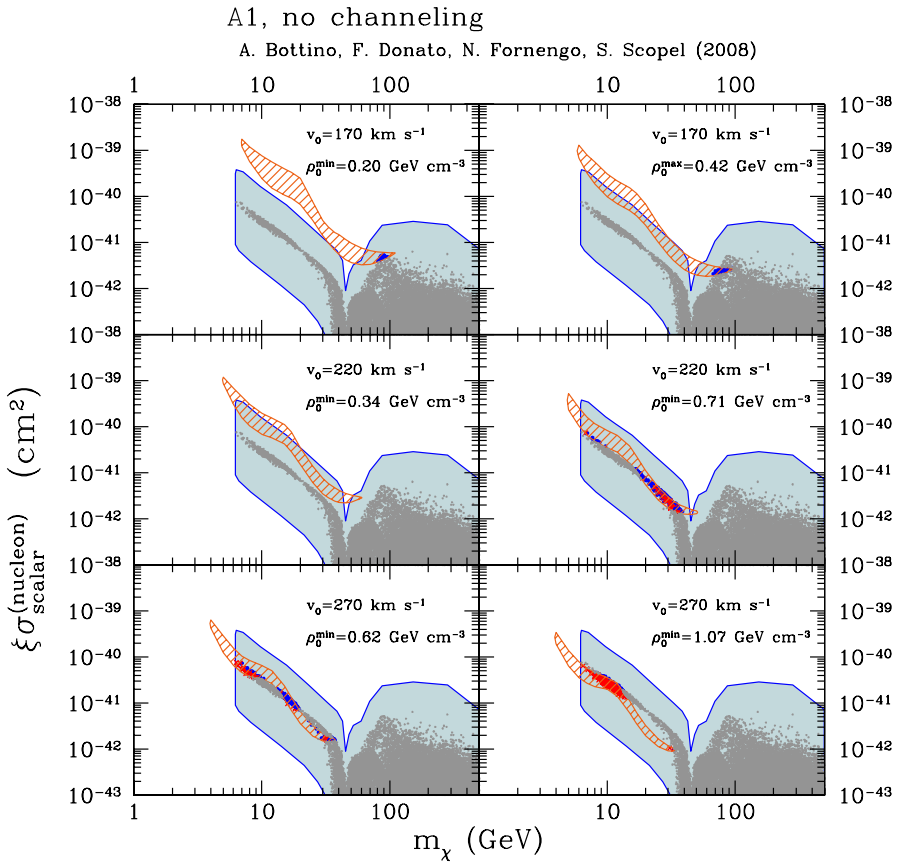


FIG. 3 (color online). $\xi\sigma_{\rm scalar}^{\rm (nucleon)}$ as a function of the WIMP mass. The region covered by a (red) slant hatching denotes the DAMA annual-modulation region, under the hypothesis that the effect is due to a WIMP with a coherent interaction with nuclei and *without including* the channeling effect. This region represents the domain where the likelihood-function values differ by more than $6.5\sigma$ from the null hypothesis (absence of modulation). It has been derived by the DAMA Collaboration by assuming that the WIMP distribution function is given by the cored-isothermal sphere (denoted as the Evans logarithmic model, or the A1 model, in Ref. [19]) and using the parameters of set A of Sec. 7.2 of the first paper of Ref. [3]. The scatter plot and the (blue) uniformly shaded region are as in Fig. 1.

downwards, when the hadronic uncertainties reported in Eq. (14) are included. The range of the pion-nucleon sigma term of Eq. (13) is responsible for the upper extension of the physical region, as compared to the representative scatter plot, by an enhancement factor of about 2–3, whereas the range of Eq. (12) generates the lower extension by a suppression factor of order 8–9. These numbers follow immediately from the formulas in Sec. III C, by taking into account that the dominant term in the quantity $I_{h,H}$ is the one involving $g_d$. Thus, the scatter plot for any set of values of hadronic quantities with given values of $g_d$ and $g_u$ can *approximately* be obtained from the one corresponding to the reference set of values, characterized by $g_{u,\mathrm{ref}} = 123$ MeV, $g_{d,\mathrm{ref}} = 290$ MeV, by scaling the reference scatter plot by the factor $(g_d/g_{d,\mathrm{ref}})^2$. However, notice that, in deriving the boundaries of the full theoretical region in Figs. 1 and 2, the full expression of Eq. (9) has been used.

From Figs. 1 and 2 it is clear that the DAMA annual-modulation region is largely compatible with the theoretical predictions for relic neutralinos with masses $m_\chi \lesssim 100$ GeV, in particular, for neutralinos within the low-energy funnel for $m_\chi \lesssim 50$ GeV. This occurs whether or not the channeling effect is included.

### B. Annual-modulation regions for single halo models

We turn now to the analysis of the annual-modulation regions for specific forms of the WIMP distribution function. First we discuss in detail our reference model, the cored-isothermal sphere, mentioned in Sec. III A (denoted as the Evans logarithmic model, or the A1 model, in Ref. [19]); we will comment about some other DFs afterwords.

Figures 3 and 4 display the theoretical predictions of our supersymmetric model (already shown in Figs. 1 and 2) together with the DAMA annual-modulation regions [56], under the hypothesis that the WIMP-nucleus interaction is coherent and that the velocity DF is given by the cored-isothermal sphere. The various insets refer to the representative values of $v_0$ and $\rho_0$ discussed before, that is, (i) $v_0 = 170$ km sec$^{-1}$ with $\rho_0^{\mathrm{min}} = 0.20$ GeV cm$^{-3}$ and $\rho_0^{\mathrm{max}} = 0.42$ GeV cm$^{-3}$; (ii) $v_0 = 220$ km sec$^{-1}$ with $\rho_0^{\mathrm{min}} = 0.34$ GeV cm$^{-3}$ and $\rho_0^{\mathrm{max}} = 0.71$ GeV cm$^{-3}$; and (iii) $v_0 = 270$ km sec$^{-1}$ with $\rho_0^{\mathrm{min}} = 0.62$ GeV cm$^{-3}$ and

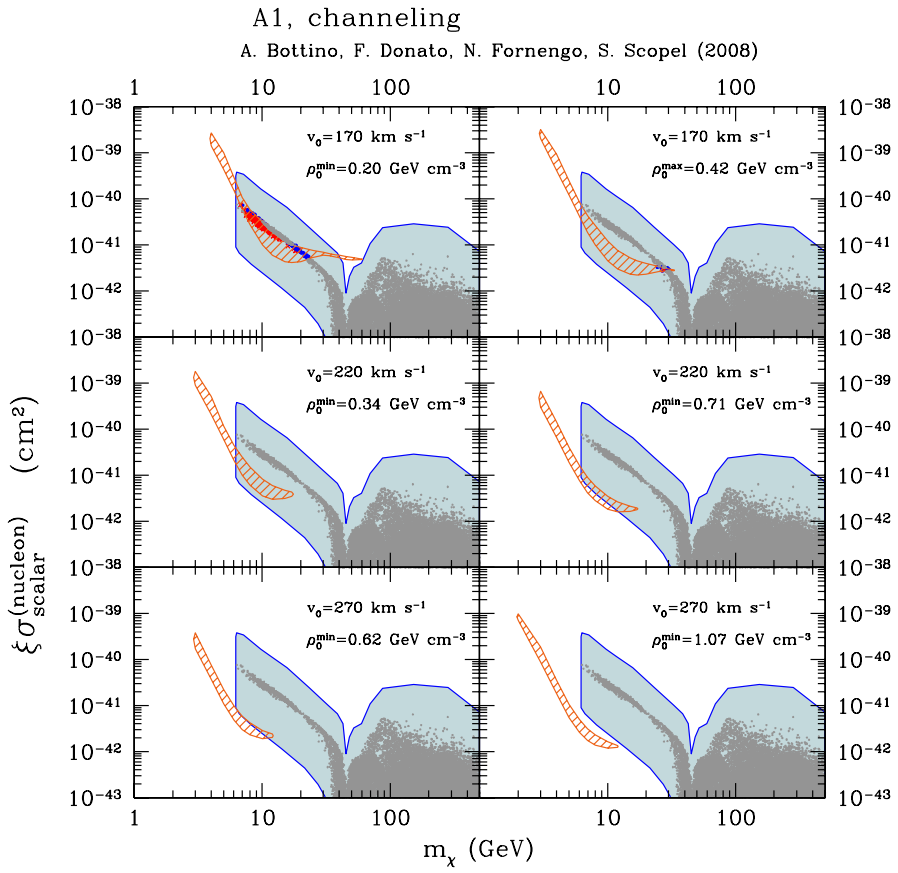


FIG. 4 (color online). $\xi\sigma_{\mathrm{scalar}}^{(\mathrm{nucleon})}$ as a function of the WIMP mass. The region covered by a (red) slant hatching denotes the DAMA annual-modulation region, under the hypothesis that the effect is due to a WIMP with a coherent interaction with nuclei and *including* the channeling effect. All other prerequisites of this region are as in Fig. 3. The scatter plot and the (blue) uniformly shaded region are as in Fig. 1.

$\rho_0^{\max} = 1.07$ GeV cm$^{-3}$. $v_{esc}$ is set to the value $v_{esc} = 650$ km sec$^{-1}$.

These DAMA annual-modulation regions represent domains where the likelihood-function values differ by more than $6.5\sigma$ from the null hypothesis (absence of modulation). The notations for the various regions and for the scatter plot are the same as in Figs. 1 and 2; Fig. 3 refers to the case in which the channeling effect is not included, and Fig. 4 to the case where channeling is included.

It is remarkable that relic neutralinos are able to provide a good fit to the experimental data. In the case of no channeling, low values of $v_0$ and $\rho_0$ ($v_0 \simeq 170$ km sec$^{-1}$ and $\rho_0 \simeq 0.2$ GeV cm$^{-3}$) appear to be somewhat disfavored, though in this case neutralinos with $m_\chi \simeq$ 60–100 GeV could be involved. The agreement between experimental data and theoretical evaluations in our model looks very good for the other combinations of $v_0$ and $\rho_0$ values, with an overall preference for neutralinos of low mass. For the case where the channeling is included according to the modeling of Ref. [7], experimental data favor values of $v_0$ and $\rho_0$ which are in the low-medium side of their own physical ranges, i.e. $v_0 \simeq$ (170–220) km sec$^{-1}$ and $\rho_0 \simeq$ (0.3–0.4) GeV cm$^{-3}$, and neutralino masses in the mass range $m_\chi \simeq$ (7–30) GeV.

When no rotation of the halo is considered, the features of the annual-modulation region in the $m_\chi - \xi\sigma_{\rm scalar}^{\rm nucleon}$ plane do not differ much when the Galactic DF is varied among many of the Galactic DFs considered in Ref. [19]. For instance, for a matter density with a Navarro-Frenk-White profile (the A5 model of Ref. [19]) or for an isothermal model with a nonisotropic velocity dispersion (the B1 model of Ref. [19]), the physical situations are very similar to the ones depicted in Figs. 3 and 4.

However, in the case of DFs with triaxial spatial distributions (within class D of Ref. [19]) and for models with a corotating halo, there can be an elongation of the annual-modulation region towards heavier masses (these are generic characteristic features which can be derived from the analysis of Ref. [19]). These features are displayed in Figs. 1 and 2 for masses up to the value of 100 GeV, which corresponds to the upper extreme of the annual-modulation region provided up to now by the DAMA Collaboration.

We wish to recall that the distribution of WIMPs in the Galaxy could deviate from the models mentioned above, mainly because of the presence of streams. For modification of the annual-modulation region in these instances, see Refs. [3,58].

## V. UPPER BOUNDS ON THE WIMP-NUCLEON SCALAR CROSS SECTION

Other experiments of WIMP direct detection, different from DAMA/NaI and DAMA/LIBRA, do not currently have the capability of measuring the annual-modulation effect; they can only provide upper bounds for the expected signals [1,4–6]. Once a specific form for the WIMP DF is taken and the relevant parameters fixed, these bounds can be converted into constraints on the WIMP-nucleus cross section. It is obvious that, in order to derive solid constraints on the WIMP physical properties, a conservative approach has to be followed in the selection of the WIMP distribution function; i.e. among the wide variety of DFs, one has to select the ones which imply the smallest responses in the detector.

As an example, we take the data recently published by the CDMS Collaboration [5]. From these data, applied to a WIMP with a coherent interaction with nuclei, one can derive the upper bounds for the quantity $\xi\sigma_{\rm scalar}^{\rm (nucleon)}$ displayed in Fig. 5, for a number of various DFs. The strong dependence of the upper bounds on the assumed DF is apparent. Superimposed on these limits is our theoretical region for relic neutralinos. We note that the conservative upper bound, established by the B1 distribution function, does not exclude any of the light neutralino configurations, when the hadronic uncertainties are taken into account

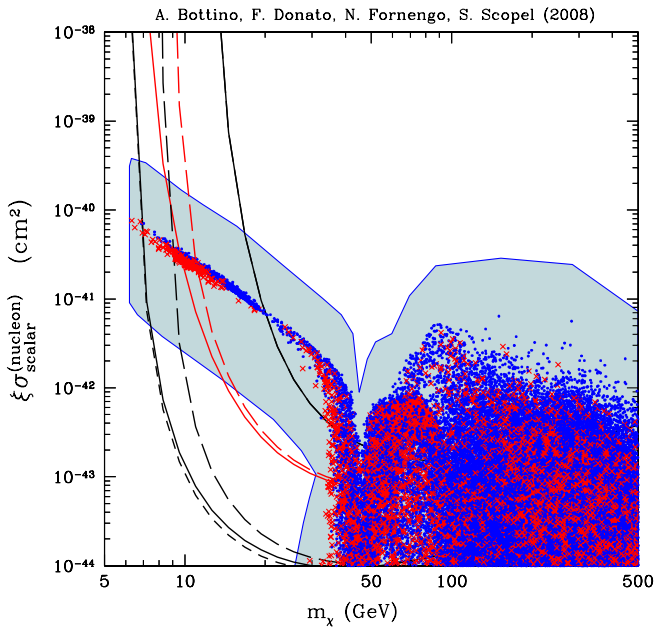


FIG. 5 (color online). The solid lines show the upper limit on the quantity $\xi\sigma_{\rm scalar}^{\rm (nucleon)}$ as a function of the WIMP mass $m_\chi$ for the CDMS detector [5] and for $v_{esc} = 650$ km sec$^{-1}$. The (red) middle line refers to the standard isothermal sphere with $v_0 =$ 220 km sec$^{-1}$ and $\rho_0 = 0.3$ GeV cm$^{-3}$ (model A0 of Ref. [19]). The (black) upper and lower curves refer to model B1 with $v_0 =$ 170 km sec$^{-1}$ (upper solid line) and model C3 with $v_0 =$ 270 km sec$^{-1}$ (lower solid line). The short-dashed line refers to model C3 with maximal counterrotation of the Galactic halo. The long-dashed lines show the upper limits for CDMS in the case of a lower escape velocity $v_{esc} = 450$ km sec$^{-1}$: the upper line refers to model A1, the lower one to model C3. For model B1, the limit coincides with the corresponding solid line. The scatter plot and the (blue) uniformly shaded region are as in Fig. 1. Other specifications are in the text.

(only some configurations with neutralino masses above 60 GeV are excluded). Of course, other WIMP distribution functions, such as the isothermal sphere, would introduce constraints on the supersymmetric population.

However, one has to notice that the aforementioned bounds are obtained through involved procedures for discriminating electromagnetic signals from recoil events and through delicate subtractions meant to separate putative WIMP signals from neutron-induced events. A major critical point in these experiments and related analyses is that the very signature (the annual modulation) of the searched signal cannot be employed in extracting the authentic events. Possible problems of stability in the acquisition parameters can affect the rejection procedures applied to a large number of events, as well as the determination of the threshold and of the energy scale [59]. In view of possible sizable uncertainties involved in these procedures, we conservatively do not implement the upper bounds discussed in this section, while comparing theoretical expectations for relic neutralinos to the annual-modulation data of Ref. [2].

It is also worth noting that the upper bounds of Ref. [5], even when taken at their face value, are however not in conflict with the annual-modulation data *and* the theoretical neutralino interpretation for masses $\sim$7–10 GeV. Compatibility of the DAMA/LIBRA annual-modulation results with the upper bounds of other experiments for coherently interacting WIMPs with the masses $\lesssim 10$ GeV is also found in the two papers [60,61], which appeared concomitantly with the present article.

Finally, we recall that another experiment (KIMS [6]), running at present with a detector of about 104 kg of CsI crystals, is meant to provide a measurement of the WIMP annual modulation in the future.

## VI. GALACTIC ANTIPROTONS

In Secs. IV A and IV B we have seen that the agreement of the DAMA data with theoretical evaluations for relic neutralinos is quite good for light neutralino masses and for wide intervals of the astrophysical quantities $\rho_0$ and $v_0$ within the ranges discussed in Sec. III A. However, it turns out that the data of cosmic antiproton fluxes can put stringent limits on light neutralino configurations [46,62].

In fact, in Ref. [63] it is shown that the experimental antiproton spectrum is fitted very well by the secondary component from cosmic ray spallation, calculated with the set of diffusion parameters which is derived from the analysis of the boron-to-carbon ratio (B/C) component of cosmic rays [64]. Indeed, the calculated secondary flux of cosmic antiprotons fits the experimental data with a $\chi^2 = 33.6$ with 32 data points, and with an uncertainty of 20%. This means that very little room is left for a possible primary component of antiprotons generated by an exotic origin (neutralino self-annihilation in our case).

Let us recall that in Ref. [63] the secondary antiproton spectrum, generated by spallation processes, was propagated using a two-zone diffusion model described in terms of five parameters. Two of these parameters, $K_0$ and $\delta$, enter the expression of the diffusion coefficient: $K = K_0 \beta R^\delta$ ($R$ is the particle rigidity); the other three parameters are the Alfén velocity $V_A$, the velocity of the convective wind $V_c$, and the thickness $L$ of the two large diffusion layers which sandwich the thin Galactic disk [64]. When studying the primary antiprotons, one can extract the following three sets of propagation parameters: the best-fit (on B/C) set (denoted as the median), together with the sets which yield the minimal and the maximal primary antiproton fluxes [65]. The values of these three sets are given in Table I.

We proceed now to analyze the extent of compatibility of the neutralino configurations which fit the DAMA results with the present data on cosmic antiprotons. Among the six sets of values for the parameters $v_0$ and $\rho_0$ analyzed in Figs. 3 and 4, let us consider the following ones (the same ones already considered in Ref. [46]): A) $v_0 = 170$ km sec$^{-1}$, $\rho_0^{\min} = 0.20$ GeV cm$^{-3}$; B) $v_0 = 170$ km sec$^{-1}$, $\rho_0^{\max} = 0.42$ GeV cm$^{-3}$; C) $v_0 = 220$ km sec$^{-1}$, $\rho_0^{\min} = 0.34$ GeV cm$^{-3}$.

In Figs. 6 and 7 we give the antiproton fluxes at $\bar{p}$ kinetic energy $T_{\bar{p}} = 0.23$ GeV, as a function of the neutralino mass for a cored-isothermal halo and for the neutralino configurations selected by the DAMA regions shown in Figs. 3 and 4, respectively. Figure 6 refers to the case in which channeling is not included in the derivation of the DAMA regions, and Fig. 7 to the case with channeling included.

At variance with what is displayed in Figs. 1–5, where the scatter plot was evaluated at the reference point $g_{u,\mathrm{ref}} =$

TABLE I. Astrophysical parameters of the two-zone diffusion model for Galactic cosmic ray propagation, compatible with B/C analysis and yielding the maximal, median, and minimal primary antiproton fluxes [65].

| Case | $\delta$ | $K_0$ (kpc$^2$/Myr) | $L$ (kpc) | $V_c$ (km s$^{-1}$) | $V_A$ (km s$^{-1}$) |
|---|---|---|---|---|---|
| Maximal | 0.46 | 0.0765 | 15 | 5 | 117.6 |
| Median | 0.70 | 0.0112 | 4 | 12 | 52.9 |
| Minimal | 0.85 | 0.0016 | 1 | 13.5 | 22.4 |

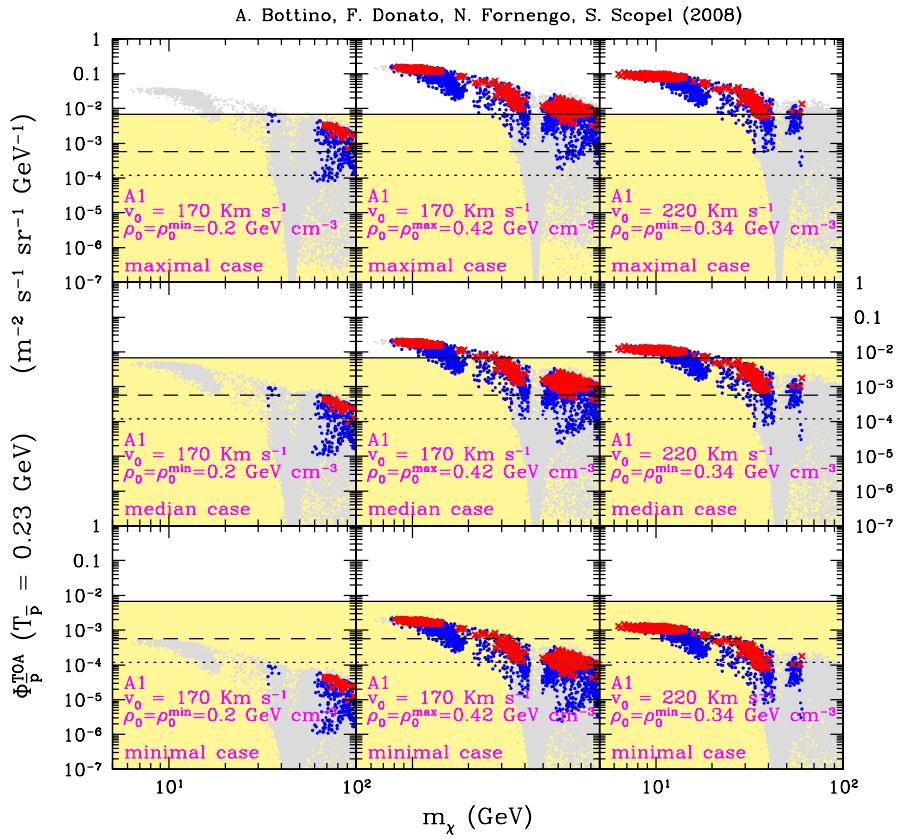


FIG. 6 (color online). Antiproton flux, at $\bar{p}$ kinetic energy $T_{\bar{p}} = 0.23$ GeV, generated by the neutralino configurations selected by the DAMA data, when a cored-isothermal halo is employed and the channeling effect is not included. Each row corresponds to a different set of cosmic ray propagation parameters: the upper, middle, and lower rows refer to the sets which provide the maximal, median, and minimal antiproton fluxes, respectively (see Table I). The three columns refer to the sets of $v_0$ and $\rho_0$ values denoted as sets $A$, $B$, and $C$ in the text. The bold (colored) points refer to configurations compatible with the DAMA regions for the case in which the channeling effect is not included (see Fig. 3). In selecting the allowed configurations the hadronic uncertainties have been taken into account. The points are differentiated as follows: (red) crosses denote configurations with a neutralino relic abundance which matches the WMAP cold dark matter amount ($0.098 \leq \Omega_\chi h^2 \leq 0.122$), while (blue) dots refer to configurations where the neutralino is subdominant ($\Omega_\chi h^2 < 0.098$). The light gray points denote configurations with a neutralino-nucleon scattering cross section outside the corresponding DAMA allowed region. The solid horizontal line shows the maximal allowable amount of antiprotons in the BESS data [66] over the secondary component; the dashed and dotted lines denote estimates of the PAMELA [67] and AMS-02 [73] sensitivities to exotic antiprotons for a 3 year mission, respectively.

123 MeV, $g_{d,\mathrm{ref}} = 290$ MeV, in Figs. 6 and 7 the scatter plots are the results not only of the scan over the supersymmetric parameter space but also of the variations of the quantities $g_u$ and $g_d$, as given by Eqs. (10) and (11), when $\sigma_{\pi N}$ and $\sigma_0$ are varied in the ranges of Eqs. (14) and (15), respectively, and $r$ is put at the default value $r = 25$.

From the results shown in Figs. 6 and 7 we see that, though a number of configurations are excluded by the BESS data [66], many others are perfectly compatible with BESS and, in principle, accessible to PAMELA [67] and AMS-02 [68]. More specifically, for set $A$, most of the neutralino configurations are unconstrained by the Galactic antiproton data, except for a group of them in the case of the maximal set of diffusion parameters and when channeling is included; a sizable number of configurations are at the level of possible investigation. Sets $B$ and $C$, due to their corresponding higher values of $\rho_0$, are more sensitive to the $\bar{p}$ constraints (but also, to a large extent, accessible to PAMELA and AMS), though prevalently for sets of the diffusion parameters close to the maximal set.

It is worth noticing explicitly that for the other sets of $v_0$ and $\rho_0$ discussed in Sec. IV B and in Figs. 3 and 4, but not considered here, one would obtain plots similar to the ones displayed in Figs. 6 and 7 with scatter plots rescaled according to the power $\rho_0^2$; thus for these sets the $\bar{p}$ constraints would be more severe than in the previous cases.

As we noticed above, a sizable number of neutralino configurations are at the level of the sensitivities of current experiments on cosmic antimatter. However, for the reasons explained above, the corresponding primary fluxes would be rather difficult to disentangle from the secondary flux (notice that primary and secondary fluxes also have

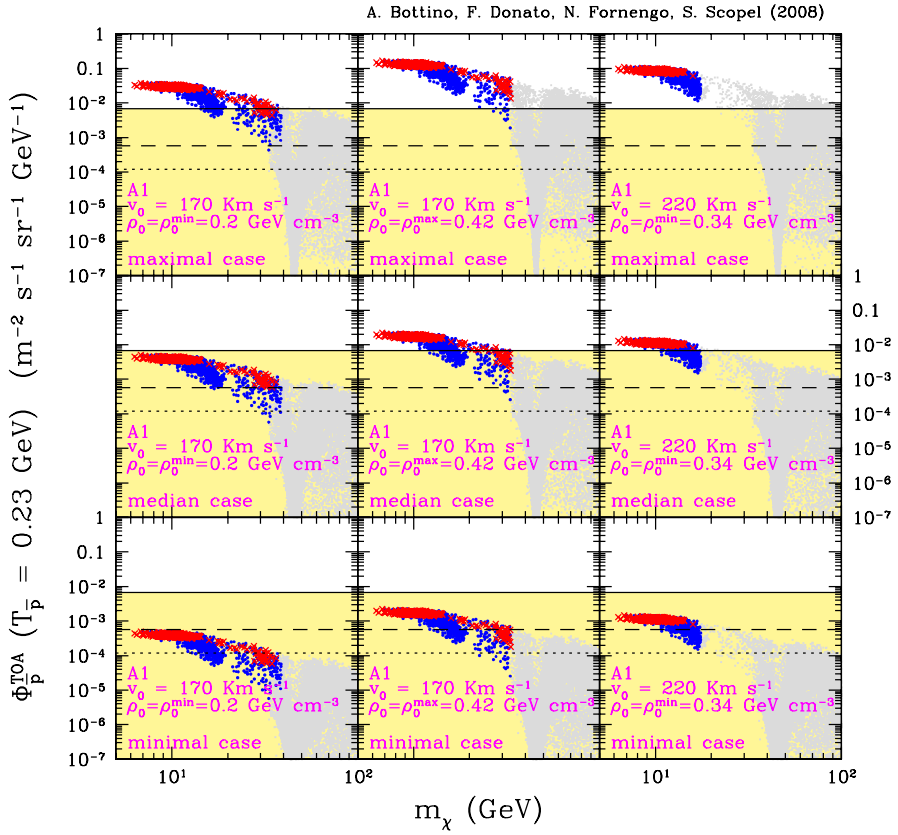


FIG. 7 (color online). Antiproton flux, at $\bar{p}$ kinetic energy $T_{\bar{p}} = 0.23$ GeV, generated by the neutralino configurations selected by the DAMA data, when a cored-isothermal halo is employed and the channeling effect is included. Notations are as in Fig. 6, except that here the neutralino configurations of the scatter plot are those selected by the DAMA regions of Fig. 4.

very similar behaviors as functions of the $\bar{p}$ kinetic energy) [65]. The cosmic antiproton data, powerful in providing stringent constraints, are somewhat problematic in providing positive signals for exotic production. The case is different for antideuterons, which we discuss in the following section.

## VII. SEARCH FOR ANTIDEUTERONS IN THE GALACTIC HALO

In Ref. [69] it was shown that the antideuteron spectra derived from DM self-annihilation are much flatter than the expected astrophysical component for kinetic energies $T_{\bar{D}} \lesssim 2$–$3$ GeV/n. Recently, the calculation of the primary and secondary antideuteron fluxes has been performed [70] in the framework of the full propagation model outlined in the previous section, encoding all the possible uncertainty sources. In Refs. [70,71] it has been shown that antideuterons offer a very promising signal for the indirect detection of intermediate and low mass DM particles by means of future detectors such as GAPS on long and ultralong duration balloon (LDB and ULDB) flights [72] and AMS-02 for three years of data taking [73].

In the present section, we present results on the fluxes of antideuterons produced from DM self-annihilation in the Galactic halo following the procedure explained in Ref. [70] (we refer to this paper for all details). In Fig. 8 we display the antideuteron flux calculated at $\bar{D}$ kinetic energy of $T_{\bar{D}} = 0.23$ GeV/n as a function of the neutralino mass for the cored-isothermal halo A1 of Eq. (3). The scatter plot represents the supersymmetric configurations selected by DAMA data when the channeling effect is not included, while Fig. 9 shows the same quantities when the channeling effect is included. The configurations have been selected with the same method as in the previous section. The three upper, middle, and lower figures correspond to the maximum, median, and minimum sets of propagation parameters of Table I. The dotted and dashed horizontal lines assess the sensitivities of AMS-02 and GAPS ULDB, respectively. The light gray (green) points correspond to supersymmetric configurations yielding an exceedingly high antiproton flux (see Figs. 6 and 7). Figures 8 and 9 show that a sizable number of neutralino configurations compatible with the annual-modulation data can generate signals accessible to antideuteron searches planned for the next years. It is notable that a bunch of configurations not accessible to antiproton signals could instead be probed by antideuteron searches.

In Fig. 10, by way of example, we show the antideuteron flux for a DM halo made of $m_\chi = 20$ GeV neutralinos

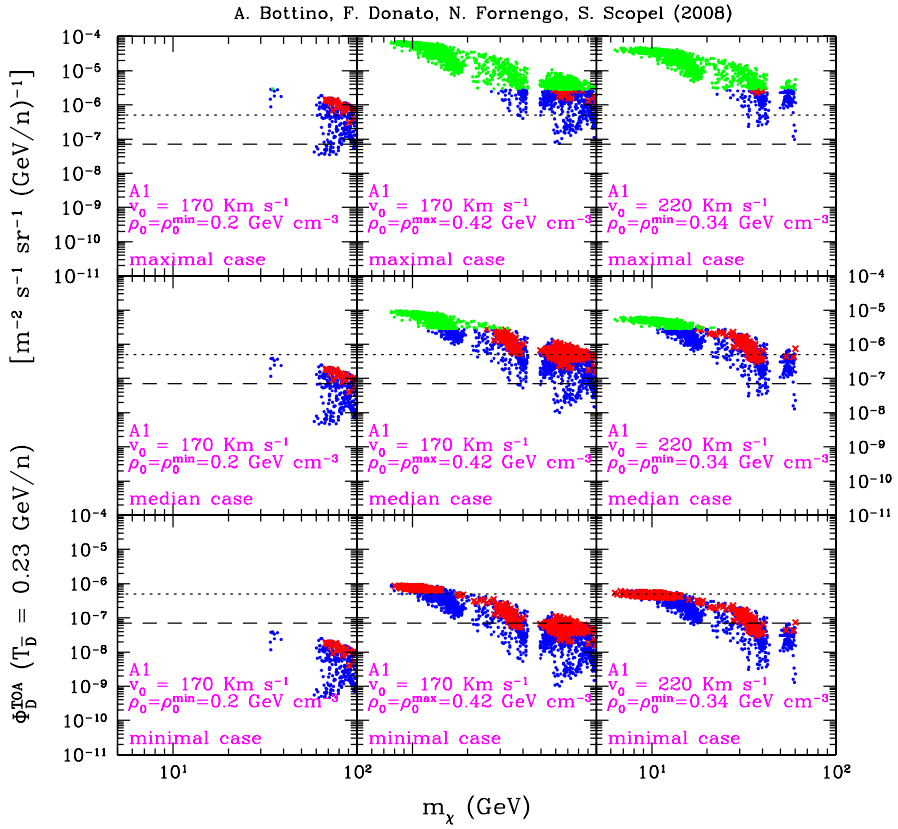


FIG. 8 (color online). Antideuteron flux, at $\bar{D}$ kinetic energy $T_{\bar{D}} = 0.23$ GeV/n, generated by neutralino configurations selected by the DAMA data when a cored-isothermal halo is employed and the channeling effect is not included. Each row corresponds to a different set of cosmic ray propagation parameters: the upper, middle, and lower rows refer to the sets which provide the maximal, median, and minimal antiproton fluxes, respectively (see Table I). The three columns refer to the sets of $v_0$ and $\rho_0$ values denoted as sets *A*, *B*, and *C* in the text. The bold (colored) points refer to configurations compatible with the DAMA regions for the case in which the channeling effect is not included (see Fig. 3). In selecting the allowed configurations the hadronic uncertainties have been taken into account. The points are differentiated as follows: (red) crosses denote configurations with a neutralino relic abundance which matches the WMAP cold dark matter amount ($0.098 \leq \Omega_\chi h^2 \leq 0.122$), while (blue) dots refer to configurations where the neutralino is subdominant ($\Omega_\chi h^2 < 0.098$). The light gray (green) points denote supersymmetric configurations yielding an exceedingly high antiproton flux (see Fig. 6). The horizontal lines refer to estimated sensitivities to antideuterons of the GAPS (dashed) and AMS (dotted) detectors.

compatible with the DAMA effect, with $\rho_0 = 0.34$ GeV cm$^{-3}$ and setting the propagation parameters to the median values. The lower dashed line corresponds to the secondary antideuteron flux as obtained in Ref. [70]. Fluxes are modulated at the solar minimum. The three horizontal lines are the estimated sensitivities for (from top to bottom) AMS-02, GAPS LDB, and GAPS ULDB flights. The primary flux stands well above the background and exceeds the experimental reach of next-generation detectors. The result is noticeable: both GAPS and AMS-02 will have the capability of clearly detecting antideuterons produced from a neutralino halo compatible with the positive signal found in DAMA data.

## VIII. MEASUREMENTS AT THE LHC

Naturally, the viability of the interpretation of the DAMA annual-modulation data in terms of relic neutralinos depends ultimately on the results which the LHC will provide on supersymmetric theories. A thorough investigation of the search for light neutralinos at the LHC has recently been carried out in Ref. [74]. In this paper two specific scenarios are analyzed, both of which are dictated by cosmological properties pertaining to light neutralinos.

A first scenario, scenario $\mathcal{A}$, is identified by the following sector of the supersymmetric parameter space: $M_1 \sim 10$ GeV, $|\mu| \sim$ (100–200) GeV, $m_A \sim 90$ GeV, $\tan\beta \sim$ 30–45, $-1 \lesssim A \lesssim +1$; the other supersymmetric parameters are not *a priori* fixed. In this scenario the cosmological bound $\Omega_\chi h^2 \leq (\Omega_{\rm CDM} h^2)_{\rm max}$ is satisfied because of a neutralino self-annihilation mediated by the light $A$ boson, combined with a high value of $\tan\beta$ and a sizable $b$-ino–Higgsino mixing in the neutralino composition.

A second scenario, scenario $\mathcal{B}$, is identified by the following sector of the supersymmetric parameter space: $M_1 \sim 25$ GeV, $|\mu| \gtrsim 500$ GeV, $\tan\beta \lesssim 20$,

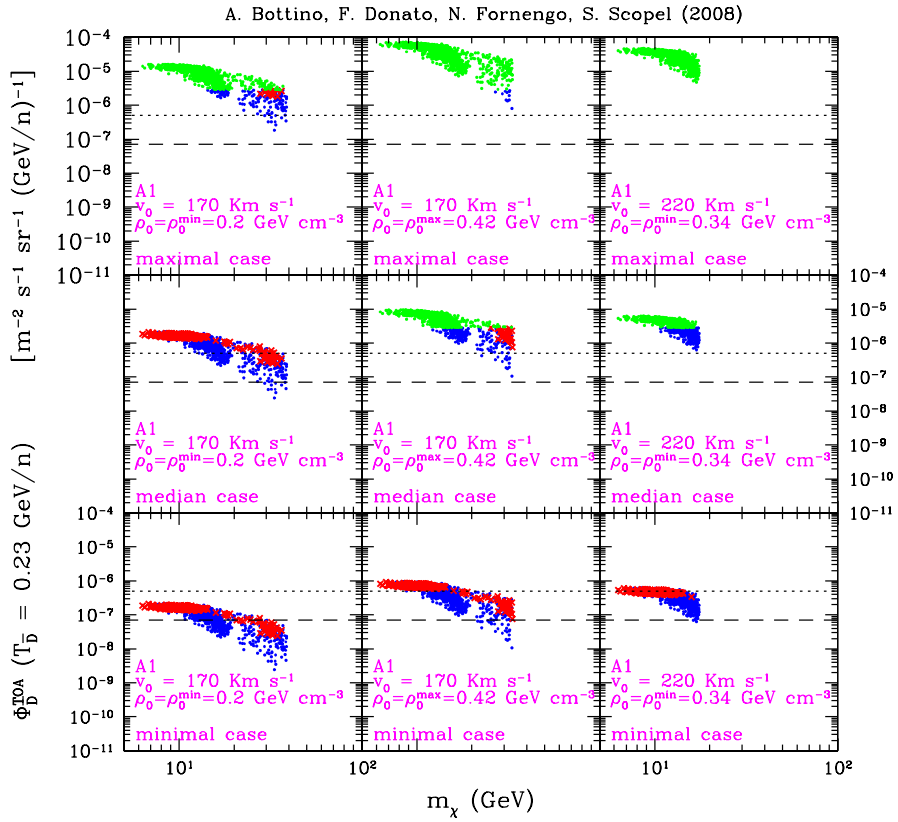


FIG. 9 (color online). Antideuteron flux, at $\bar{D}$ kinetic energy $T_{\bar{D}} = 0.23$ GeV/n, generated by neutralino configurations selected by the DAMA data when a cored-isothermal halo is employed and the channeling effect is included (see Fig. 4). The light gray (green) points denote supersymmetric configurations yielding an exceedingly high antiproton flux (see Fig. 7). Other notations are as in Fig. 8, except that here the neutralino configurations of the scatter plot are those selected by the DAMA regions of Fig. 4.

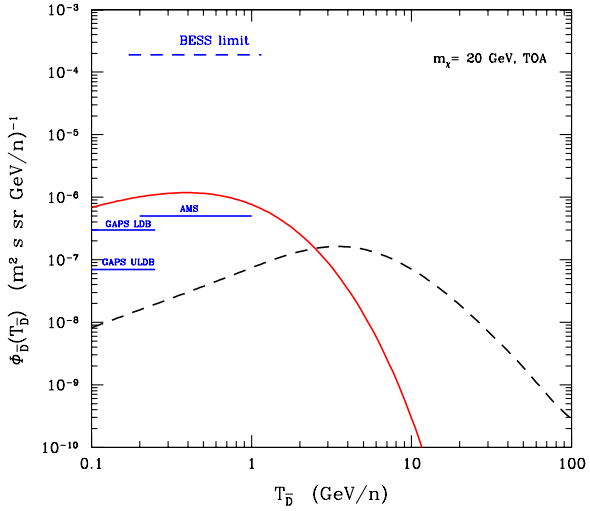


FIG. 10 (color online). Solid line: antideuteron flux for a DM halo of $m_\chi = 20$ GeV neutralinos compatible with the DAMA modulation effect. Dashed line: secondary component [70]. Propagation parameters are set at the median configuration of Table I. The upper dashed horizontal line is the present BESS upper limit on the search for cosmic antideuterons. The three horizontal solid (blue) lines are the estimated sensitivities for (from top to bottom) AMS-02, GAPS on a LDB, and GAPS on an ULDB.

$m_{\tilde{l}} \gtrsim$ (100–200) GeV, $-2.5 \lesssim A \lesssim +2.5$; the other supersymmetric parameters are not *a priori* fixed. In this case the cosmological constraint $\Omega_\chi h^2 \leq (\Omega_{\rm CDM} h^2)_{\rm max}$ is satisfied because of stau-exchange contributions (in the $t$, $u$ channels) to the neutralino self-annihilation cross section.

In Ref. [74] the signals expected at the LHC in the two scenarios are discussed through the main (sequential and branched) chain processes, started by a squark produced in the initial proton-proton scattering. Branching ratios and the expected total number of events are derived in the various benchmarks defined within the two scenarios.

On the basis of these results, it is proved in Ref. [74] that the LHC should allow an efficient exploration of the supersymmetric parameter regions compatible with light neutralinos. Because of the characteristic features of these regions, the measurements of the LHC should be able to prove or disprove the supersymmetric model considered in the present paper and then validate or not our interpretation of the annual-modulation effect in terms of relic neutralinos.

## IX. CONCLUSIONS

In this paper we have analyzed the most recent experimental data on direct searches for dark matter particles in

the Galactic halo. We have discussed the various features involved in an interpretation of these data in terms of relic neutralinos; the supersymmetric scheme employed is an effective MSSM scheme at the electroweak scale, without gaugino-mass unification at a grand-unified-theory scale. The role of the uncertainties affecting the neutralino-quark couplings, because of the involved hadronic quantities, is critically discussed and included in our considerations.

First we have considered in detail the results of the DAMA Collaboration which, by a combined analysis of the DAMA/NaI and the DAMA/LIBRA experiments, for a total exposure of 0.82 ton yr, provide evidence of an annual-modulation effect at $8.2\sigma$ C.L. Comparison of our theoretical evaluations with the DAMA data has been carried out both in the case in which the channeling effect is included in the DAMA analysis and in the one where it is excluded. The DAMA results presented here refer uniquely to the case in which the putative WIMP has a coherent interaction with the nuclei in the detector and are therefore translated in terms of regions in the $m_\chi - \xi\sigma_{\rm scalar}^{\rm (nucleon)}$ plane, for different selections of the Galactic distribution functions [56]. We also wish to recall that DM-detector interaction mechanisms or DM candidates different from the one considered in the present paper could be the origin of the annual-modulation effect [2].

The roles of the hadronic uncertainties and of the effect of channeling are kept separated at any stage of our discussion on DAMA data; the analysis has been carried out in such a way that, hopefully once some of the aforementioned uncertainties are resolved in the future, one can easily employ our present results to narrow down the physically relevant regions.

By considering first the DAMA data when a convolution of Galactic distribution functions is considered, we have shown that the annual-modulation region is largely compatible with the theoretical predictions for relic neutralinos with masses $m_\chi \lesssim 100$ GeV and, in particular, for neutralinos within the low-energy funnel for $m_\chi \lesssim 50$ GeV. This occurs whether or not the channeling effect is included.

We have then pursued our analysis by employing the cored-isothermal sphere DF and shown that relic neutralinos fit the annual-modulation data quite well. For the case where the channeling is included according to the modeling of Ref. [7], experimental data favor values of $v_0$ and $\rho_0$ which are in the low-medium side of their own physical ranges, i.e. $v_0 \simeq (170\text{–}220)$ km sec$^{-1}$ and $\rho_0 \simeq (0.3\text{–}0.4)$ GeV cm$^{-3}$, and neutralino masses in the mass range $m_\chi \simeq (7\text{–}30)$ GeV. In the case of no channeling, low values of $v_0$ and $\rho_0$ ($v_0 \simeq 170$ km sec$^{-1}$ and $\rho_0 \simeq 0.2$ GeV cm$^{-3}$) appear to be somewhat disfavored, though in this case neutralinos with $m_\chi \simeq 60\text{–}100$ GeV could be involved. The agreement between experimental data and theoretical evaluations looks very good for the other combinations of $v_0$ and $\rho_0$ values, with an overall preference for neutralinos of low mass. We have also commented about the results one would obtain when some other DF is selected.

The neutralino populations selected on the basis of the annual-modulation data have been analyzed in terms of the antiproton fluxes which they would produce in our halo. We have shown that many of them are fully compatible with the current stringent bounds on cosmic antiprotons, especially for values of local dark matter density $\rho_0$ and local rotational velocity $v_0$ in the low side of their physical ranges, and for values of the diffusion parameters not too close to the values of their maximal set.

It was also derived that forthcoming measurements of Galactic antideuterons will have a good chance to explore fluxes generated by the self-annihilation of the neutralino configurations compatible with the annual-modulation data.

The upper bounds on $\xi\sigma_{\rm scalar}^{\rm (nucleon)}$, derived by other experiments of WIMP direct searches [1,4–6], have been analyzed by considering various WIMP Galactic DFs and by including the uncertainties induced by the previously mentioned hadronic quantities. It is concluded that no conservative upper bound can now exclude the light ($m_\chi \lesssim 50$ GeV) neutralino population within the model discussed in Sec. II.

We have pointed out that the LHC is expected to allow an efficient exploration of the supersymmetric parameter regions compatible with light neutralinos and the annual-modulation data. Because of the characteristic features of the physical regions involved, the measurements of the LHC could be able to prove or disprove the supersymmetric model considered in the present paper and then validate or not our interpretation of the annual-modulation effect in terms of relic neutralinos.

It is finally worth noting that the relic neutralinos of light masses, considered in the present paper and previously in Refs. [9,55], can be of relevance also in many interesting astrophysical contexts different from the ones discussed before. For instance, by their self-annihilations, these neutralinos may be the origin of electron-positron pairs which could interact with photons of the cosmic microwave background producing a peculiar Sunyaev-Zeldovic effect [75,76]. Also, positrons and electrons created by annihilation of light neutralinos in the Galactic center might generate a synchrotron radiation responsible for an excess of microwave emission from a region within $\sim 20°$ of the Galactic center [77] (see also Ref. [78]). Light neutralino dark matter could also imply a sizable primordial $^6$Li abundance [79], a feature particularly interesting in view of recent new determinations of this abundance in metal-poor halo stars [80].

## ACKNOWLEDGMENTS

We thank the DAMA Collaboration for providing us with the results of their analysis prior to their publication. We are also grateful to Rita Bernabei and Pierluigi Belli

for useful discussions. We acknowledge Research Grants funded jointly by Ministero dell'Istruzione, dell'Università e della Ricerca, by Università di Torino, and by Istituto Nazionale di Fisica Nucleare within the *Astroparticle Physics Project* .

[1] For a general overview about experiments for direct detection of relic particles, see, for instance, the review talks given by P. Belli and G. Gerbier (D. Bauer) at TAUP 2007, Sendai, Japan, 2007, and the contributions presented in the relevant workshop sessions at the same conference (see http://www.awa.tohoku.ac.jp/taup2007/ and forthcoming proceedings).

[2] R. Bernabei *et al.* (DAMA Collaboration), Nucl. Instrum. Methods Phys. Res., Sect. A **592**, 297 (2008); arXiv:0804.2741 [Eur. Phys. J. C (to be published)].

[3] R. Bernabei *et al.* (DAMA Collaboration), Riv. Nuovo Cimento Soc. Ital. Fis. **26N1**, 1 (2003); Int. J. Mod. Phys. D **13**, 2127 (2004).

[4] J. Angle *et al.* (XENON Collaboration), Phys. Rev. Lett. **100**, 021303 (2008).

[5] Z. Ahmed *et al.* (CDMS Collaboration), arXiv:0802.3530.

[6] H. S. Lee *et al.* (KIMS Collaboration), Phys. Rev. Lett. **99**, 091301 (2007); S. K. Kim, contribution to the International Conference on Topics in Astroparticle and Underground Physics (TAUP) 2007 (see http://www.awa.tohoku.ac.jp/taup2007/ and forthcoming proceedings).

[7] R. Bernabei *et al.* (DAMA Collaboration), Eur. Phys. J. C **53**, 205 (2008).

[8] E. M. Drobyshevski, arXiv:0706.3095, and references quoted therein.

[9] A. Bottino, N. Fornengo, and S. Scopel, Phys. Rev. D **67**, 063519 (2003); A. Bottino, F. Donato, N. Fornengo, and S. Scopel, Phys. Rev. D **68**, 043506 (2003).

[10] A. Colaleo (ALEPH Collaboration), in Proceedings of SUSY'01, 2001, Dubna, Russia; J. Abdallah *et al.* (DELPHI Collaboration), Report No. DELPHI 2001-085 CONF 513, 2001; LEP Higgs Working Group for Higgs boson searches, arXiv:hep-ex/0107029; LEP2 Joint SUSY Working Group, http://lepsusy.web.cern.ch/lepsusy/.

[11] A. A. Affolder *et al.* (CDF Collaboration), Phys. Rev. Lett. **86**, 4472 (2001); V. M. Abazov *et al.* (D0 Collaboration), Phys. Rev. Lett. **97**, 171806 (2006).

[12] E. Barberio *et al.* (HFAG), arXiv:hep-ex/0603003.

[13] M. Ciuchini, G. Degrassi, P. Gambino, and G. F. Giudice, Nucl. Phys. **B534**, 3 (1998).

[14] M. Misiak *et al.*, Phys. Rev. Lett. **98**, 022002 (2007).

[15] V. M. Abazov *et al.* (D0 Collaboration), Phys. Rev. D **76**, 092001 (2007).

[16] G. W. Bennet *et al.* (Muon $g-2$ Collaboration), Phys. Rev. D **73**, 072003 (2006).

[17] J. Bijnens and J. Prades, Mod. Phys. Lett. A **22**, 767 (2007).

[18] J. Dunkley *et al.* (WMAP), arXiv:0803.0586.

[19] P. Belli, R. Cerulli, N. Fornengo, and S. Scopel, Phys. Rev. D **66**, 043503 (2002).

[20] A. Bottino, F. Donato, N. Fornengo, and S. Scopel, Phys. Rev. D **72**, 083521 (2005).

[21] The class of models discussed in Ref. [19] represents a quite exhaustive summary of dark matter distribution functions as possible departures from the isothermal sphere model. Notice, however, that it does not include the possibility of nonthermal components in the $f(\vec{v})$, which could, in principle, modify the high-velocity tail of the velocity DF [see, for instance, A. Helmi, S. D. M. White, and V. Springel, Phys. Rev. D **66**, 063502 (2002)].

[22] For other analyses, see, for instance, A. M. Green, Phys. Rev. D **68**, 023004 (2003); **69**, 109902(E) (2004); **66**, 083003 (2002); **63**, 043005 (2001); M. Kamionkowski and A. Kinkhabwala, Phys. Rev. D **57**, 3256 (1998); J. D. Vergados, Phys. Rev. Lett. **83**, 3597 (1999); J. D. Vergados and D. Owen, Astrophys. J. **589**, 17 (2003); P. Ullio and M. Kamionkowski, J. High Energy Phys. 03 (2001) 049; J. Edsjo, M. Schelke, and P. Ullio, J. Cosmol. Astropart. Phys. 09 (2004) 004; G. Gelmini and P. Gondolo, Phys. Rev. D **63**, 036006 (2001).

[23] C. S. Kochanek, Astrophys. J. **457**, 228 (1996).

[24] M. Feast and P. Whitelock, Mon. Not. R. Astron. Soc. **291**, 683 (1997).

[25] T. K. Gaisser, G. Steigman, and S. Tilav, Phys. Rev. D **34**, 2206 (1986).

[26] R. Barbieri, M. Frigeni, and G. F. Giudice, Nucl. Phys. **B313**, 725 (1989).

[27] K. Griest, Phys. Rev. D **38**, 2357 (1988); Nucl. Phys. **B313**, 725 (1989).

[28] A. Bottino, F. Donato, N. Fornengo, and S. Scopel, Phys. Rev. D **59**, 095003 (1999).

[29] A. Bottino, F. Donato, N. Fornengo, and S. Scopel, Astropart. Phys. **18**, 205 (2002).

[30] M. A. Shifman, A. I. Vainshstein, and V. I. Zacharov, Phys. Lett. **78B**, 443 (1978); JETP Lett. **22**, 55 (1975).

[31] A. Bottino, F. Donato, N. Fornengo, and S. Scopel, Astropart. Phys. **13**, 215 (2000).

[32] A. Bottino, V. de Alfaro, N. Fornengo, A. Morales, J. Puimedon, and S. Scopel, Mod. Phys. Lett. A **7**, 733 (1992).

[33] G. Jungman, M. Kamionkowski, and K. Griest, Phys. Rep. **267**, 195 (1996).

[34] J. Ellis, A. Ferstl, and K. A. Olive, Phys. Lett. B **481**, 304 (2000).

[35] E. Accomando, R. Arnowitt, B. Dutta, and Y. Santoso, Nucl. Phys. **B585**, 124 (2000).

[36] A. Corsetti and P. Nath, Phys. Rev. D **64**, 125010 (2001).

[37] J. L. Feng, K. T. Matchev, and F. Wilczek, Phys. Lett. B **482**, 388 (2000).

[38] J. Ellis, K. A. Olive, and C. Savage, Phys. Rev. D **77**, 065026 (2008).

[39] R. Koch, Z. Phys. C **15**, 161 (1982).

[40] J. Gasser, H. Leutwyler, and M. E. Sainio, Phys. Lett. B **253**, 260 (1991).

[41] M. M. Pavan, R. A. Arndt, I. I. Strakovsky, and R. L. Workman, PiN Newslett. **16**, 110 (2002).
[42] SAID pion-nucleon database, http://gwdac.phys.gwu.edu/.
[43] M. G. Olsson, Phys. Lett. B **482**, 50 (2000).
[44] L. Chang, Y. Liu, and H. Guo, Phys. Rev. D **72**, 094023 (2005).
[45] J. Gasser and H. Leutwyler, Phys. Rep. **87**, 77 (1982).
[46] A. Bottino, F. Donato, N. Fornengo, and S. Scopel, Phys. Rev. D **77**, 015002 (2008).
[47] A. K. Drukier, K. Freese, and D. N. Spergel, Phys. Rev. D **33**, 3495 (1986); K. Freese, J. A. Frieman, and A. Gould, Phys. Rev. D **37**, 3388 (1988).
[48] R. Bernabei *et al.*, Int. J. Mod. Phys. A **21**, 1445 (2006); **22**, 3155 (2007); arXiv:0802.4336 [Mod. Phys. Lett. A (to be published)]; Phys. Rev. D **77**, 023506 (2008).
[49] R. Tucker-Smith and N. Weiner, Phys. Rev. D **72**, 063509 (2005).
[50] R. Foot, Phys. Rev. D **78**, 043529 (2008).
[51] C. Arina and N. Fornengo, J. High Energy Phys. 11 (2007) 29.
[52] A. Bottino, F. Donato, N. Fornengo, and S. Scopel, Phys. Lett. B **423**, 109 (1998).
[53] R. Bernabei *et al.*, Phys. Lett. B **424**, 195 (1998).
[54] A. Bottino, F. Donato, N. Fornengo, and S. Scopel, Phys. Rev. D **69**, 037302 (2004).
[55] A. Bottino, F. Donato, N. Fornengo, and S. Scopel, Phys. Rev. D **70**, 015005 (2004).
[56] DAMA Collaboration (private communication).
[57] In deriving the regions of Figs. 1 and 2, cases A, B, C defined in Sec. 7.2 of the first paper of Ref. [3] have been included.
[58] R. Bernabei *et al.*, Eur. Phys. J. C **47**, 263 (2006).
[59] For a survey on features of liquid noble gas detectors, see R. Bernabei, P. Belli, A. Incicchitti, and D. Prosperi, arXiv:0806.0011.
[60] J. L. Feng, J. Kumar, and L. E. Strigari, arXiv:0806.3746.
[61] F. J. Petriello and K. M. Zurek, arXiv:0806.3989.
[62] A. Bottino, F. Donato, N. Fornengo, and P. Salati, Phys. Rev. D **72**, 083518 (2005).
[63] F. Donato *et al.*, Astrophys. J. **563**, 172 (2001).
[64] D. Maurin, F. Donato, R. Taillet, and P. Salati, Astrophys. J. **555**, 585 (2001).
[65] F. Donato *et al.*, Phys. Rev. D **69**, 063501 (2004).
[66] T. Maeno *et al.* (BESS Collaboration), Astropart. Phys. **16**, 121 (2001).
[67] M. Boezio *et al.*, Nucl. Phys. B, Proc. Suppl. **134**, 39 (2004); P. Picozza and A. Morselli, arXiv:astro-ph/0604207.
[68] S. Ahlen *et al.*, Nucl. Instrum. Methods Phys. Res., Sect. A **350**, 351 (1994).
[69] F. Donato, N. Fornengo, and P. Salati, Phys. Rev. D **62**, 043003 (2000).
[70] F. Donato, N. Fornengo, and D. Maurin, Phys. Rev. D **78**, 043506 (2008).
[71] H. Baer and S. Profumo, J. Cosmol. Astropart. Phys. 12 (2005) 008.
[72] C. J. Hailey *et al.*, J. Cosmol. Astropart. Phys. 01 (2006) 007; J. Koglin, contribution to "The Hunt for Dark Matter," Fermilab, 2007.
[73] V. Choutko and F. Giovacchini, on behalf of the AMS Collaboration, Proceedings of the 30th International Cosmic Ray Conference, Merida, Mexico, 2007.
[74] A. Bottino, N. Fornengo, G. Polesello, and S. Scopel, Phys. Rev. D **77**, 115026 (2008).
[75] S. Colafrancesco, Astron. Astrophys. **422**, L23 (2004).
[76] S. Colafrancesco, P. de Bernardis, S. Masi, G. Polenta, and P. Ullio, arXiv:astro-ph:0702568.
[77] D. P. Finkbeiner, arXiv:astro-ph/0409027; D. Hooper, D. P. Finkbeiner, and G. Dobler, Phys. Rev. D **76**, 083012 (2007); D. Hooper, Phys. Rev. D **77**, 123523 (2008).
[78] A. Bottino, F. Donato, N. Fornengo, and S. Scopel, Phys. Rev. D **77**, 127301 (2008).
[79] K. Jedamzik, Phys. Rev. D **70**, 083510 (2004).
[80] M. Asplund *et al.*, Astrophys. J. **644**, 229 (2006).